Non-polymeric Nanogels as Versatile Nanocarriers. Intracellular Transport of the Photosensitizers Rose Bengal and Hypericin for Photodynamic Therapy

Ana Torres-Martínez,[a] Begoña Bedrina,[a] Eva Falomir,[a] María J. Marín,[b] César A. Angulo-Pachón,[a] Francisco Galindo[a,*] and Juan F. Miravet[a,*]

[a]Departament de Química Inorgànica i Orgànica, Universitat Jaume I, Avda. Sos Baynat s/n, 12071 Castelló de la Plana, Spain. E-mail: francisco.galindo@uji.es , miravet@uji.es

[b]School of Chemistry, University of East Anglia, Norwich Research Park, Norwich NR4 7TJ, UK

ABSTRACT

The use of nanocarriers for intracellular transport of actives has been extensively studied in recent years and represents a central area of Nanomedicine. The main novelty of this paper lies on the use of nanogels formed by a low molecular weight gelator (**1**). Here, non-polymeric, molecular nanogels are successfully used for intracellular transport of two photodynamic therapy (PDT) agents, Rose Bengal (RB) and Hypericin (HYP).

The two photosensitizers (PSs) exhibit different drawbacks for their use in clinical applications. HYP is poorly water-soluble, while the cellular uptake of RB is hindered due to its dianionic character at physiological pH values. Additionally, both PSs tend to aggregate precluding an effective PDT. Despite the different nature of these PSs, nanogels from gelator **1** provide, in both cases, an efficient intracellular transport into human colon adenocarcinoma cells (HT-29) and a notably improved PDT efficiency, as assessed by confocal laser scanning microscopy and flow cytometry. Furthermore, no significant dark toxicity of the nanogels is observed, supporting the biocompatibility of the delivery system. The developed nanogels are highly reproducible due to their non-polymeric nature and their synthesis is easily scaled up. The results here presented confirm thus the potential of molecular nanogels as valuable nanocarriers, capable of entrapping both hydrophobic and hydrophilic actives, for PDT of cancer.

Keywords: nanogels, organic molecular nanoparticles, nanovehicles, photodynamic therapy, drug delivery, nanomedicine, Rose Bengal, Hypericin

Nanomedicine, which uses biocompatible nanoparticles for diagnosis, delivery or sensing purposes,[1,2] has received extensive interest in recent years as demonstrated by the increasing number of publications engaging with this topic. For example, more than 100 review papers were published in 2019 containing the term "Nanomedicine" in the title. Nanomedicine constitutes a vast area of research due to the wide variety of nanoparticles that can be employed and the many therapeutic targets that can be introduced. A common approach in Nanomedicine is to use nanocarriers for the intracellular delivery of molecular or macromolecular bioactive species. Examples include liposomes,[3] solid-lipid nanoparticles,[4] polymeric micelles[5] and nanogels,[6] polymer-drug conjugates,[7] albumin[8] and silica nanoparticles.[9] Despite the large number of potential nanomedicines reported in the literature, only a few tens of them have been approved by the FDA for clinical use due to the many pitfalls found in the translation from bench to clinical practice.[10,11]

Conventional polymeric nanogels (nanohydrogels), nanoparticles formed by polymeric networks that retain large quantities of water, have received extensive interest in recent years due to their potential for biomedical applications.[6,12-17] Following the initial work from Vinogradov, the vast majority of nanogels consist of covalently crosslinked networks.[18,19] Alternatively, examples of physically crosslinked nanogels have also been reported in the literature and include those formed by the self-assembly of amphiphilic block copolymers,[20] hydrophobized polysaccharides[21] or DNA.[22]

Lately, our group has been interested in the study of molecular nanogels, namely nanogels, formed by aggregation of small molecules instead of polymers.[23-25] The use of molecular nanogels aims to solve some critical drawbacks of polymeric nanogels in their use as biomedical carriers,[26] such as biodegradability, stimuli responsiveness, polymer

polydispersity, and batch-to-batch reproducibility. Interestingly, nanogels constituted by low molecular weight species have an apparent relationship to their macroscopic counterparts, supramolecular (molecular) gels, which are soft materials formed by self-assembled fibrillar networks widely studied in recent decades.[27-30]

Nanocarriers are used for therapeutic applications being cancer the central area of interest.[1,31] In relation to this paper, photodynamic therapy (PDT) has been clinically used for the treatment of solid tumors for the past 25 years.[32] PDT treatment involves a systemically or topically administered photosensitizer (PS) followed by site-specific irradiation of the PS with the appropriate wavelength to generate reactive oxygen species (ROS).[33-35] Site-specific irradiation causes cancerous cells to perish while sparing healthy tissues and organs, so PDT avoids the frequent systemic severe toxicity and adverse effects of other treatments.[36,37] The mechanism to generate ROS consists of light absorption by the PS to yield the first excited state, ^{1}PS*, and then, after intersystem crossing, the excited triplet state, ^{3}PS*. The latter is quenched by oxygen present in the medium ($^{3}O_2$) generating singlet oxygen ($^{1}O_2$), *via* type II mechanism (energy transfer), and other cytotoxic species such as radical anion superoxide ($O_2^{\cdot-}$), hydroxyl radical (·OH) or hydrogen peroxide (H_2O_2), *via* type I mechanism (electron transfer).[38-41] The use of nanoparticles or nanocomposites for PDT has received increasing attention in recent years.[42-48] In this paper, we specifically address the application of molecular nanogels for the delivery of PSs with the aim of improving the PDT efficiency of the actives.

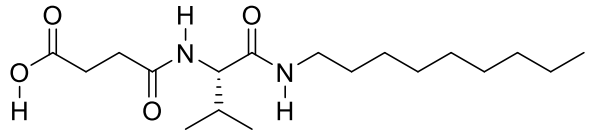

1

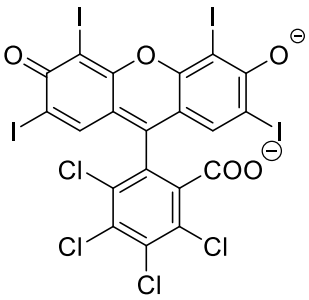

Rose Bengal, dianionic form (RB)

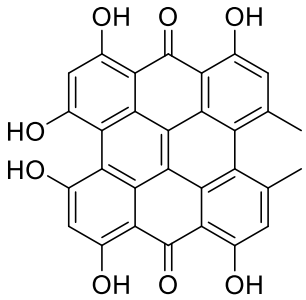

Hypericin (HYP)

Scheme 1. Chemical structure of hydrogelator **1**, Rose Bengal and Hypericin.

Rose Bengal (RB, Scheme 1) is a water-soluble, well-studied synthetic dye that absorbs strongly around 550 nm. It sensitizes the formation of $^1O_2$ with a high quantum yield ($\Phi(^1O_2)$ = 0.75 under 540 nm light irradiation), being a potent photosensitizer for type II PDT.[49,50] RB is versatile and applicable to a wide range of fields, from photocatalysis[51,52] to biomedicine. In this latter context, RB has had a profound impact as a therapeutic agent, with promising results in preclinical studies as PS for PDT treatment of cancer and the prevention of infectious diseases spreading.[53-57] Besides, its long history of safe use in systemic diagnosis of hepatic function,[58] as well as in ophthalmology,[59] has facilitated RB to advance into different clinical trials.[60-62] An essential drawback in the therapeutic use of RB is that, at physiological pH, the predominant species is a dianion, which is inhibited from crossing cell membranes and suffers from poor intracellular uptake ability.[63,64] The incorporation of the dye into nanocarriers has proved to overcome this limitation and, also, does not interfere in the photodynamic efficiency of RB.[65,66] For example, a favored intracellular accumulation,

and an enhanced phototoxic effect were achieved for RB loaded into silica nanoparticles (oral and breast cancer cells),[67] cationic dendrimers (basal carcinoma cells),[68] and covalently bond to gold nanoparticles (oral cancer cells).[69] Higher phototoxicity was also reported for RB incorporated into silica nanoparticles (skin cancer cells),[70] chitosan microcapsules (breast cancer),[71] zinc oxide nanoparticles (cervical cancer cells),[72] albumin (lung cancer cells)[73] and PAMAM dendrimers (Dalton's lymphoma ascites cells).[74]

The other PS studied here, Hypericin (HYP, Scheme 1), is a polyphenolic molecule obtained from the plant St John's Wort (*Hypericum perforatum*) with a broad pharmacological spectrum. It has an absorption maximum at *ca.* 590 nm and is also an efficient photosensitizer.[75,76] Upon light activation, both type I[77] and type II[50] mechanisms have been proposed to explain its PDT activity.[78] Additional processes have been suggested as contributors of its phototoxicity, as the formation of hypericin radicals or a hypericin-induced pH drop.[79] Some advantages of the photosensitizing activity of HYP are its minimal or no dark toxicity[80] and its preferential accumulation in neoplastic tissues.[81] The HYP-PDT antineoplastic efficacy for cancer treatment has been demonstrated in several *in vitro* and *in vivo* studies,[76] and three clinical trials for various skin disorders.[82-84] The light-dependent fungicidal, bactericidal and antiviral effects of HYP have also been reported.[85-87] A critical drawback in the clinical application of HYP in PDT comes from its low water solubility.[88,89] Furthermore, HYP tends to form non-fluorescent aggregates in aqueous media, which show a suppressed photodynamic activity and, therefore, low phototoxicity on cells.[90-93] Several HYP nanocarriers have been investigated aiming to overcome these limitations. For example, encapsulated HYP in polylactic acid nanoparticles[94] or copolymer micelles[95] showed improved intracellular accumulation in ovarian tumor animal models; solid-lipid

nanoparticles were useful as HYP transporters into cervical adenocarcinoma cells;[96] and HYP encapsulated into block copolymers[97] and calcium phosphate nanoparticles[98] improved the *in vitro* antimicrobial and antileishmanial PDT, respectively. Additional recent examples include HYP loaded in proteins[99,100] graphene oxide[101] and composite nanoparticles.[102]

It has been stated that the use of nanocarriers is the defining characteristic of the so-called third generation of PSs.[103,104] Ideally, these nanosystems should incorporate the PS without loss or alteration of the sensitizer activity.[105] Here, we address the use of a novel nanocarrier, molecular nanogels, for the improvement of cellular uptake of RB and HYP and, thus, improvement of their PDT effect. As abovementioned, these molecules present opposite physicochemical nature, high polarity and water solubility for RB, and low polarity and poor aqueous solubility for HYP, which, in both cases, leads to drawbacks for their use in clinical PDT. Results presented here highlight the versatility of the molecular nanogels used as carriers, which enhance cellular uptake of the sensitizers favoring their activity as PDT agents.

RESULTS AND DISCUSSION

The preparation of the molecular nanogels from gelator **1** ((*S*)-4-((3-methyl-1-(nonylamino)-1-oxobutan-2-yl)amino)-4-oxobutanoic acid, see Scheme 1) was previously reported in detail by our group. These particles have a gel-like nature as they are constituted mainly by water, according to static light scattering measurements.[24] Scheme 2 outlines the preparation of photosensitizer-loaded nanogels (PS@**1**) carried out in this work. In the first step, a gel of **1** in toluene is formed in the presence of the corresponding PS. Solvent removal under vacuum gave a xerogel film that was suspended, with sonication, in PBS (pH 7) to afford a colloid containing PS@**1** nanoparticles.

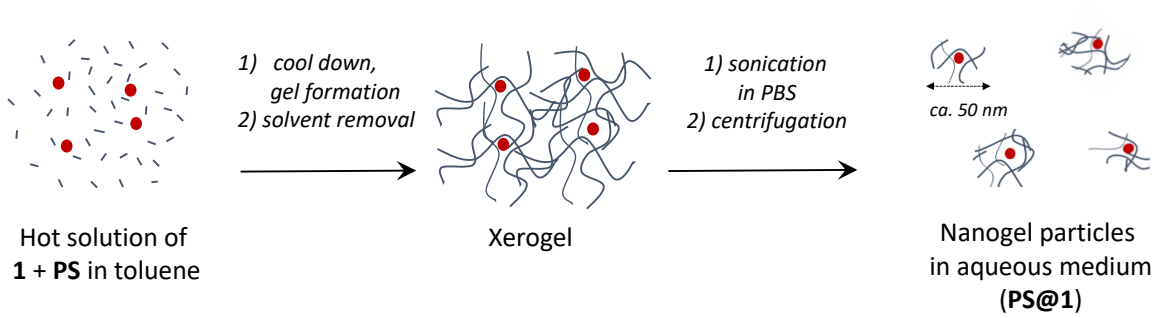

Scheme 2. Pictorial representation of the process followed to prepare PS@**1** nanogels.

Rose Bengal loaded nanogels.

Although RB is insoluble in toluene due to its ionic character, the gelator facilitated its dispersion in toluene. A related behavior has recently been reported by us for the same system in dichloromethane.[106] Therefore, homogenous gels in toluene containing RB could be prepared by cooling down to room temperature a hot solution containing **1** (7.3 mM) and RB (40 μM). Following the procedure described above (xerogel formation and sonication), a colloid containing RB-loaded nanogels, RB@**1** was obtained. The same protocol used to obtain RB@**1** was repeated without **1**, investigating how the different steps could affect the RB. It was confirmed that the photosensitizer remained stable throughout the procedure.

The analysis of the RB@**1** samples by UV-Vis spectroscopy (Figure 1) showed that the maximum absorption red-shifted from 549 nm for free RB to *ca*. 560-570 nm for the RB@**1** species in PBS. This red-shift indicates RB being in a less polar environment in the nanogel than the one found in a conventional water solution. The strong solute-solvent interactions of RB with water, which stabilize the ground state of the PS, would be perturbed in the more hydrophobic environment of the nanogel. This type of effect diminishes the energy gap between the frontier orbitals, leading to λ_{max} red-shifts in the absorption spectrum.[107,108]

Similar bathochromic shifts have been reported due to the incorporation of RB in the hydrophobic environments of micelles,[108] liposomes,[109,110] peptides,[111,112] silica nanoparticles,[70] polystyrene,[113] dendrimers[114] or self-assembled microparticles,[25] among others. It has to be noted that the mentioned shift indicates that a significant amount of RB is loaded in the nanogel particles, but the presence of free RB in the system can not be discarded. A 10 nm bathochromic shift was also observed for the maximum of the fluorescence emission spectra of the RB@**1** samples (from *ca.* 570 nm to *ca.* 580 nm).

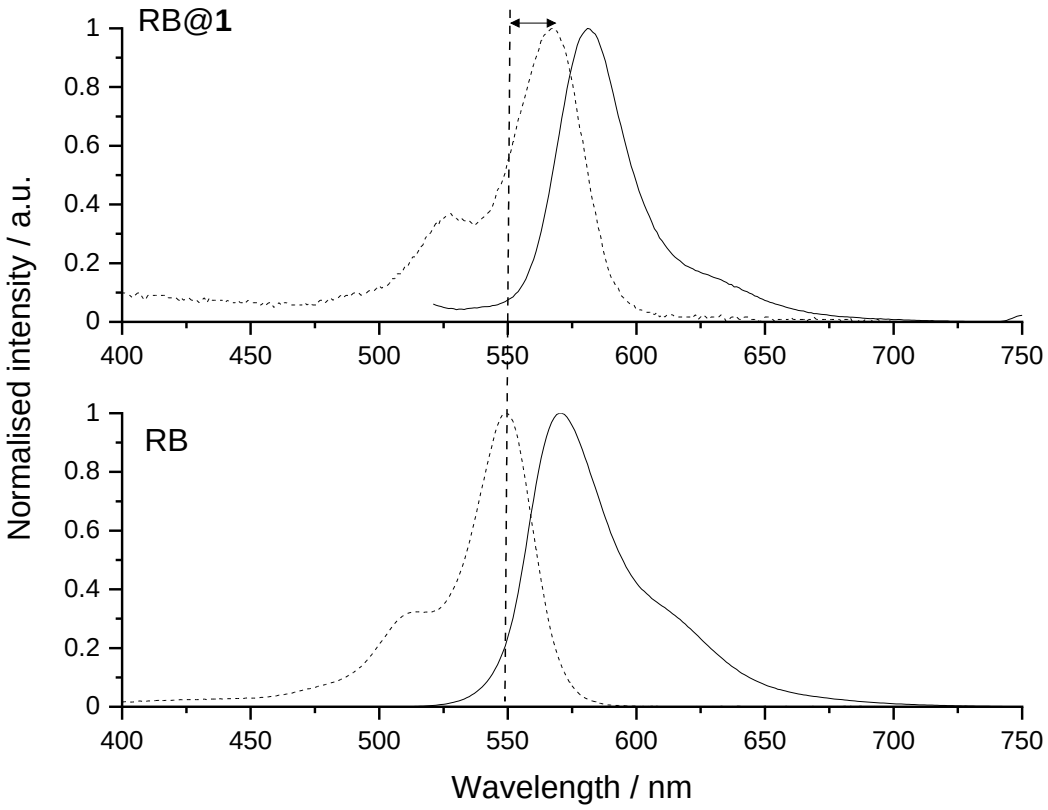

Figure 1. Normalized UV-Vis absorbance (dashed line) and fluorescence emission (solid line, λ_{ex} 500 nm) spectra for a representative RB@**1** sample (top) and RB in PBS (bottom).

RB tends to aggregate in dimers and higher multimers, a phenomenon that is detrimental for its use in PDT as ROS yields are reduced;[115] and this aggregation can be estimated from the intensity ratio of the shoulder to the maximum peak in the absorption spectrum.[110] The intensity ratio for RB@**1** is almost identical to the ratio of a free RB standard solution in PBS, in which RB is in monomeric form.

The amount of RB in these samples was determined by UV-Vis spectroscopy. The absorption at the maximum intensity wavelength was used to calculate the concentration of RB, based on a linear calibration constructed for free RB in PBS. It has to be noted that nanogel particles originate considerable light dispersion, resulting in a notable increase of the absorption baseline of the spectrum. For this reason, the quantification of RB was performed from baseline-corrected spectra (see Figures S1-S2.). The results obtained in this way were coincident with those achieved by nanogel disassembly by the addition of DMSO. The concentration of RB in RB@**1** nanogel samples was found to present some variation in the different batches with an average value of 6 ± 3 μM, which represents a drug loading of 0.8 %w/w (the concentration of **1** in the samples was determined to be 0.7 mg/mL[24]). For control purposes, in the following experiments, RB solutions in PBS with the same concentration present in RB@**1** samples were used.

RB@**1** nanoparticles were characterized by dynamic light scattering (DLS) and transmission electron microscopy (TEM) (see Figure 2). DLS revealed a number averaged diameter (D_n) of 218 nm (std dev = 6, polydispersity index = 0.24). Aging for 24 h or 1:3 dilution in the cell culture medium did not modify the size distribution significantly. Z-potential was determined to be -33.9 mV (std dev = 4.1, see Figure S15). This value indicates colloidal

stability towards aggregation, and the negative value reflects the ionizable nature of the carboxylic acids, which should be in part as carboxylates in the nanogel.

Regarding TEM, spherical and spherulitic objects were observed, which, as proposed previously,[24] would indicate that the nanogels would correspond to nucleation points that, in more concentrated solutions, would yield self-assembled fibrillar networks. The size of the particles observed by TEM is in good agreement with that obtained by DLS.

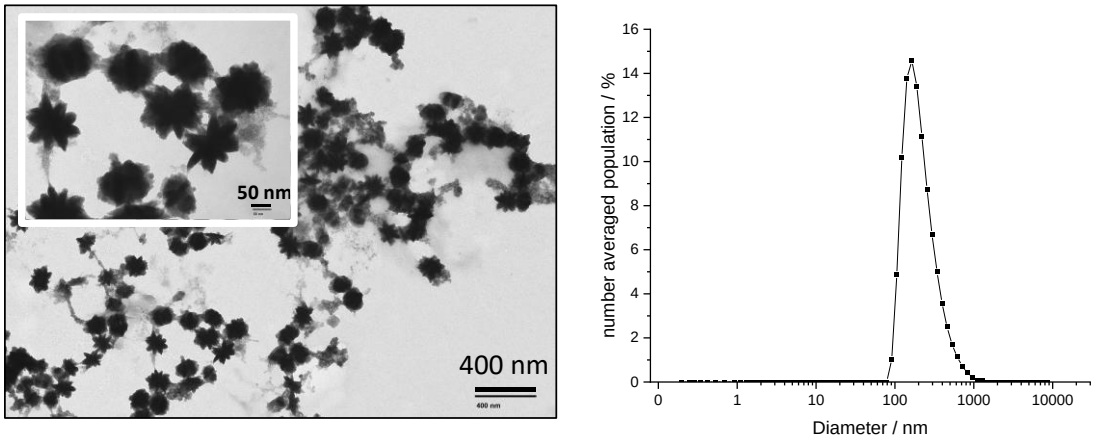

Figure 2. Analysis of RB@**1** particles. TEM images (left) and number averaged diameter distribution obtained by DLS (right).

Samples were diluted 1:3 in medium and tested in human colon adenocarcinoma cells (HT-29). This dilution was chosen because preliminary assays with **1,** using the Trypan blue exclusion test, revealed that a 1:3 dilution of the nanoparticles with medium presented negligible cytotoxicity, slightly increased for a 1:2 dilution (see Figure S3). It has to be noted the medium refers to Dulbecco's modified Eagle's medium (DMEM) used without the addition of Phenol Red to avoid interferences in optical measurements and, in the cases indicated in the Methods section, without fetal bovine serum to promote starvation.

The incorporation of RB in the cells was studied using confocal laser scanning microscopy (CLSM) and flow cytometry after a 24 h incubation period with RB@**1** nanogels. The solvent used to prepare the nanogels (PBS, pH 7) was used as the negative control. As shown in Figure 3, the confocal microscopy analysis (λ_{ex} 514 nm) of cells incubated with RB@**1** or free RB shows homogenous fluorescence intensity revealing a non-specific distribution of the PS within the cytoplasm. Previous reports indicate that RB accumulates in membranes of normal cells but it has been localized in lysosomes of melanoma cell lines.[60,63,116,117] The apparent intensity of intracellular fluorescence measured by CLSM is notably higher for the cells treated with RB@**1** nanogels than for those treated with RB alone. Flow cytometry analysis is entirely consistent with this observation. Three different nanogel batches were tested in duplicate, and the mean cell fluorescent intensity (λ_{ex} 488 nm) over negative control for the RB@**1** samples was found to be *ca.* 70 times higher than that for the free RB solutions. Such difference should not be ascribed to the interaction of RB with the nanocarrier, which increases only moderately RB fluorescence.

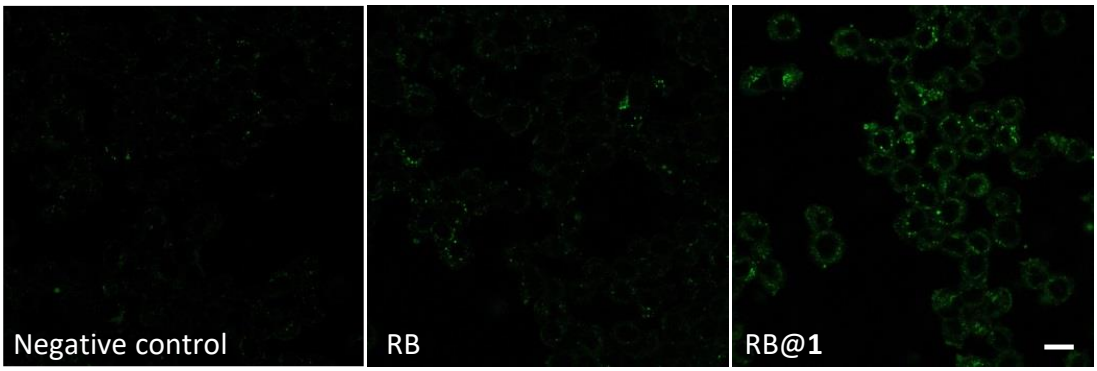

Figure 3. Confocal laser scanning microscopy images of HT-29 cells incubated for 24 h with free RB and RB@**1** nanogels (λ_{ex} 514 nm). Negative control corresponds to cells incubated with PBS. [RB] = 1.1 μM. Scale bar =16 μm.

As previously mentioned, the low cellular uptake of free RB is ascribed to its anionic character, resulting in reduced cellular membrane permeation.[63,118] The photosensitizer entrapped in nanogels of **1** would act as stealth RB. Some authors have metaphorically coined this strategy 'a Trojan horse approach'.[119] Presumably, the enhanced cellular uptake is a consequence of differences in the mechanism of RB internalization. Endocytosis, a common mechanism described for internalization of nanosized particles, probably participates in the case of the nanometric gel particles.[120]

The potential use of the RB@**1** nanogels for PDT was also investigated. HT-29 cells were incubated for 24 hours with either RB@**1** nanogels or free RB in PBS and subjected to irradiation with a white light source (two light-emitting diodes (LEDs) 11W power each one, λ_{em} = 400-700 nm) for 2 minutes. A negative control experiment was performed with HT-29 cells incubated with PBS and irradiated under the same conditions. The cell apoptosis and viability were studied 24 h after the irradiation. It has to be noted that once cells enter in contact with ROS, different mechanisms of cell death are triggered, being necrosis and apoptosis the best known. Apoptosis is a gene-directed cell suicide process undergone when cells become damaged or are no longer needed. Necrosis has been considered a passive form of cell death occurring as a consequence of physical or chemical attack to the cell. Necrosis and apoptosis are very distinct morphologically since the former is accompanied by cellular and organelle swelling, membrane breakdown, and content release to the extracellular space,[121] while apoptosis involves cell shrinkage and blebbing of the plasma membrane.[122,123] A third mechanism, autophagy, is a predominantly cytoprotective process that has been linked to both necrosis and apoptosis death, serving either as a pro-survival or pro-death function.[124] Finally, it must be recalled that the emerging paraptosis death mechanism is

gaining increasing attention within the PDT community,[125] and could also play a role in explaining the activities of our systems. However, its study is out of the scope of this research. Elucidating which mechanism is operating in the cellular death provides useful information for the rationalization and improvement of PDT.[126,127]

In the study of RB@**1** PDT activity, viability and apoptosis were evaluated by flow cytometry using a commercial kit that double-stains the cell population. Apoptosis was inferred by staining with FITC-Annexin V, which detects externalized phosphatidylserine, a feature of the early phases of apoptosis. Viability was detected with propidium iodide, which signals the loss of membrane integrity that accompanies the later stages of cell death. Three different batches of RB@**1** nanogels were tested in duplicate, and the results are summarized in Figure 4 (see dot plot at Figure S13). RB@**1** internalization results in a dramatic enhancement of the measured PDT activity when compared to the cells treated with free RB and with PBS. These findings are in accordance with the higher efficiency of cellular uptake of RB@**1** than that of free RB. RB@**1** produces an apoptotic induction or more than 70% of the cell population. In comparison, the percentage of apoptotic cells for HT-29 cells incubated with free RB close to the basal level of 15% observed for PBS control. Only apoptosis was observed as a cell death mechanism, both in staining and scattering analysis of flow cytometry data. This result is in agreement with a previous report that also finds apoptosis to be the preferred mechanism of cell death using RB.[128] Regarding dark toxicity, no significant increase in cell death was observed when the cells were incubated under the same conditions as those indicated in Figure 4 but were not subject to irradiation (Figure S4) thus, confirming the biocompatibility of the RB@**1**. The phototoxicity of unloaded nanogels was also

investigated using flow cytometry, and no cell death was observed when HT-29 cells were incubated with nanogels without RB and irradiated for 2 min (Figure S5).

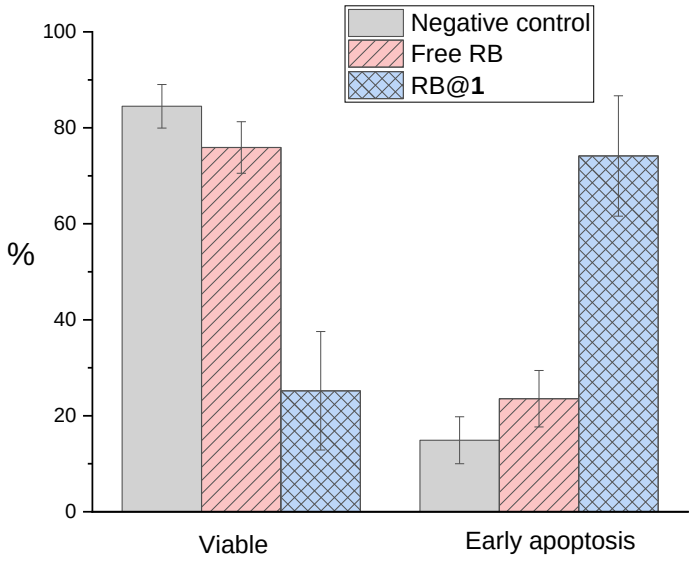

Figure 4. Results obtained by flow cytometry of cell viability and early apoptosis in PDT experiments (2 min irradiation) with HT-29 cells and RB as a photosensitizer. Annexin V-FITC/propidium iodide was used for staining. Negative control corresponds to cells incubated with PBS. The results are the average of three different batches analyzed in duplicate (average [RB] in culture media was 2 μM).

Comparison with precedent *in vitro* studies using other nanocarriers has only a relative value considering the different types of cells examined and experimental conditions. The use of RB-loaded cationic dendrimers resulted in an induction of apoptosis to 40-60% of different basal carcinoma cells.[68] In another example, organically modified mesoporous silica nanoparticles loaded with RB reduced *ca.* 40% cell proliferation in a skin cell cancer culture compared to the control.[70]

As RB is a type II photosensitizer, the photogeneration of $^1O_2$ in aqueous solutions of RB@**1** was spectroscopically measured using 9,10-anthracenediyl-bis(methylene)dimalonic acid (ABDA) as $^1O_2$ chemical trap, which is a water-soluble probe for this ROS.[129] It was observed that the entrapment of RB in the nanogel reduces moderately the rate of $^1O_2$ production, being the kinetic constants measured 8.8 and 22.5 $mM^{-1}\cdot min^{-1}$for RB@**1** and RB, respectively (Figure S6). A possible rationale for this behavior is that the nanogel environment lowers the diffusion rate of O_2 *inside* the nanogel, and consequently, the diffusion of $^1O_2$ *outside* of the nanoparticle.[130] Also, it has to be noted that the efficiency of $^1O_2$ generation *in cuvette*, hence in the absence of cells, could not be reflecting the situation in the biological context since once the RB@**1** system crosses the cellular membrane, the PS could be released due to the disassembly of the nanoparticle.

Hypericin loaded nanogels

Hypericin-loaded nanogels (HYP@**1**) were obtained from a gel of **1** in toluene formed in the presence of HYP (25 μM), which is soluble in hot toluene in the μM range of concentrations used in this experiment. As described in Scheme 2, solvent removal affords a xerogel, which is sonicated in PBS to form a sample of HYP@**1** nanogels. As shown in Figure 5, the absorption spectrum of HYP@**1** exhibits two well-defined peaks in the range 525-625 nm, with the dominance of the red-most band. However, the absorption spectrum of HYP in PBS shows a broadening of visible bands and less vibronic structure (Figure S7). These data suggest that the monomeric form of HYP is present in the nanogels. In contrast, aggregates are formed in the absence of nanoparticles. Similar absorption spectra, ascribable to the monomeric form of HYP, have been previously reported for the incorporation of this molecule in membranes, nanoparticles or proteins.[96,99,100,131-134] As for fluorescence, HYP@**1**

in PBS shows a fluorescence emission spectrum with band maxima at 597 and 647 nm while HYP in PBS shows no fluorescence under the same conditions. These results also point to the presence of free HYP in the nanogels and aggregated, non-emissive, HYP in the aqueous medium.

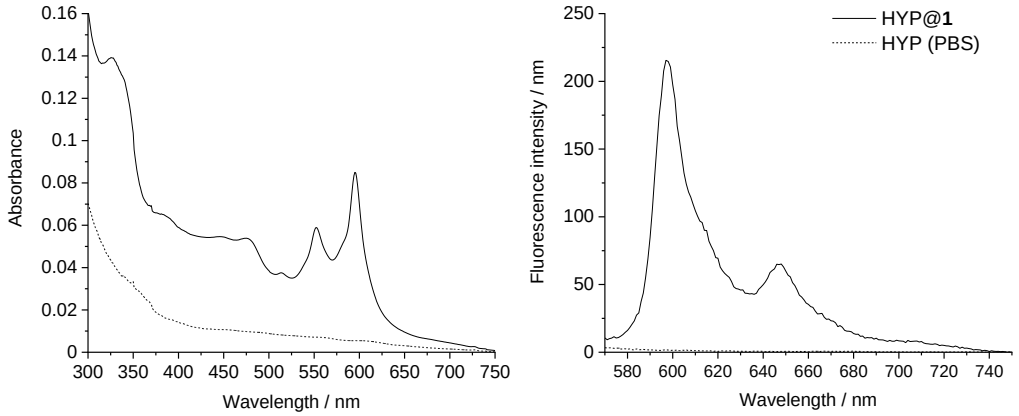

Figure 5. UV-Vis absorption and fluorescence emission (λ_{ex} 550 nm) spectra of a representative HYP@**1** sample (solid line) and HYP in PBS.

A blue-shift going from HYP in DMSO to HYP@**1** in PBS is detected both for absorption and emission maxima (Figure S7; 599 to 596 nm and 603 to 597 nm, respectively). This maxima displacement indicates that the environment of HYP in the nanogels presents reduced polarity compared to DMSO.[135] Hypericin could be establishing π-π interactions with hydrophobic areas or hydrogen bonds with the gelator molecules, as has been suggested for other systems.[136]

The quantification of HYP in the nanogel samples was performed by UV-Vis spectroscopy. The absorption at the maximum intensity wavelength was used to calculate the concentration of HYP, based on a linear calibration made from free HYP in DMSO. As in the case of RB@**1**, HYP@**1** nanogel particles originate considerable light dispersion, and quantification

of HYP was performed from baseline-corrected spectra (see Figure S2). The results obtained in this way were coincident with those achieved by nanogel disassembly by the addition of DMSO. An average loading of 0.7 ± 0.3 μM of HYP (0.05 %w/w drug loading) was obtained. Similar loadings were reported for other HYP-encapsulated systems.[97,132,134,137-140] Samples prepared as HYP@**1** nanogels but without the addition of gelator were used as a control (HYP in PBS from here on). The maximum concentration of HYP that can be solubilized in PBS by this method was 0.09±0.05 μM, which is one order of magnitude lower than the solubility in the presence of the nanogels.

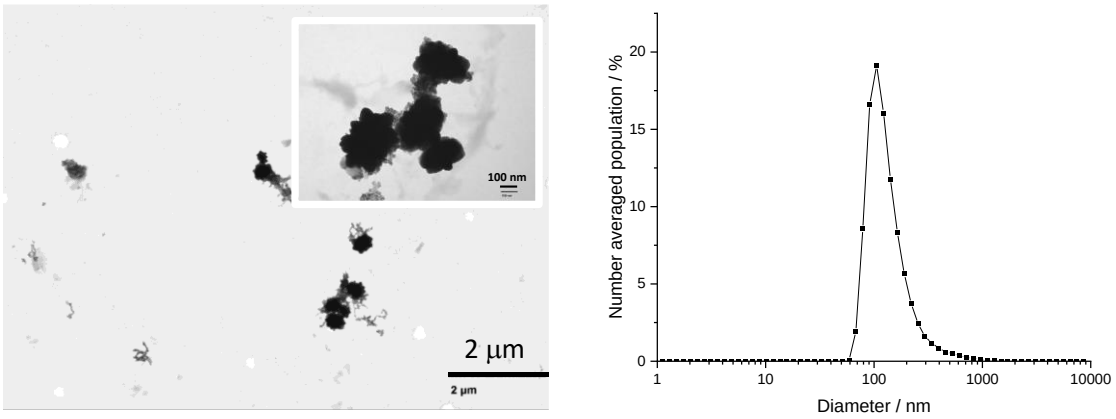

Figure 6. Analysis of HYP@**1** particles. TEM images (left) and number averaged diameter distribution obtained by DLS (right).

HYP@**1** nanoparticles were characterized by dynamic light scattering (DLS) and transmission electron microscopy (TEM) (see Figure 6). The results are similar to those obtained for RB@**1** samples regarding both morphology and sample stability. DLS revealed a number averaged diameter (D_n) of 137 nm (std dev = 7, polydispersity index = 0.32). Aging for 24 h or 1:3 dilution in the cell culture medium did not modify the size distribution

significantly. Additionally, the Z-potential was similar to that measured for RB@**1**, with a value of -36.1 mV (std dev = 1.8, see Figure S16).

The cellular uptake of HYP@**1** by HT-29 cells was also studied using flow cytometry and confocal laser scanning microscopy similarly as described above for RB@**1**. HT-29 cells were incubated for 24 h with HYP@**1** nanogels and the average fluorescence emission per cell measured by flow cytometry was used as an indicator of the internalization of HYP. Due to the very low solubility of HYP in PBS, control samples at the same concentration were prepared using 1% v/v DMSO as co-solvent (from here on, PBS-DMSO). However, PBS without any DMSO was used as the solvent for the samples with HYP@**1**. Flow cytometry analysis of three different nanogel batches was performed in duplicate. The mean cell fluorescent intensity (λ_{ex} 488 nm) was found to be *ca.* three times higher for the HYP@**1** system than for the sample containing HYP in PBS-DMSO. Moreover, the internalization of HYP for cells incubated with HYP@**1** in PBS gave a 14 times higher fluorescence intensity than that obtained for HYP dispersed in PBS without DMSO. Care should be taken to interpret the intracellular fluorescence intensity of HYP due to the sensitivity of its emission efficiency to aggregation and polarity. It is assumed that the nanogel is disassembled in the cell, and the HYP emission from the different samples can be compared. Confocal laser scanning microscopy images (Figure 7 and S8) agree qualitatively with the flow cytometry data, indicating significantly higher emission inside the cells treated with HYP@**1** than inside cells treated with free HYP administered in PBS or in PBS-DMSO. The images reveal that HYP is preferentially accumulated in the membrane when cells are incubated with the HYP in PBS-DMSO sample (see Figure S5). However, when HYP@**1** is studied, the HYP is localized in the cytoplasm in a non-specific manner. It has been reported that HYP, due to its

pronounced hydrophobic character, accumulates in lipid membranes.[141] Noticeably, it was described that, for HeLa cells, the use of serum in the culture media with HYP led from a plasma membrane staining (with non-fluorescent aggregates in the rest of the cell) to a non-specific, cytoplasmic localization.[142] This could be the case for HYP@**1** nanoparticles, and the nanogel would play a similar role to that of the serum proteins.

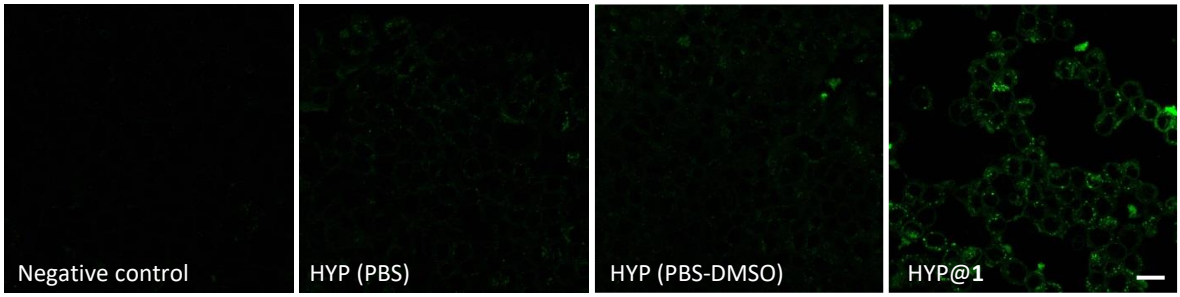

Figure 7. Images from confocal laser scanning microscopy; λ_{ex} 561 nm. Cells were incubated for 24 h with the samples. [HYP] = 0.2 μM. Scale bar = 20 μm.

The efficiency of HYP@**1** for *in vitro* PDT was also studied in HT-29 cells as described above for RB@**1**. For HYP@**1**, viability and apoptosis were detected based on changes in the permeability of cell membranes, using a commercial kit with YO-PRO®-1/propidium iodide staining. Three different batches of HYP@**1** nanogels were tested in duplicate, and the results are summarized in Figure 8 (see dot plot at Figure S14). Irradiation of cells incubated with HYP@**1** in PBS and HYP in PBS-DMSO caused in both cases a significant reduction in cell viability. For example, cell viability is *ca.*10 % for HYP@**1** and 85 % for negative controls. On the other hand, no photoactivity was found for controls using HYP in PBS without DMSO, being the percentages of viable cells near the basal level (see Figure S9). Also, low dark toxicity was observed in all cases (see Figure S10).

Irradiation of the cells in the presence of HYP@**1** shows, according to the alterations in the light scattering pattern of the cells observed by flow cytometry (Figure S14), a prevalence of necrosis over apoptosis. This effect had also been observed previously in HT-29 cells treated with HYP and exposed to an extensive range of PDT doses.[143] Protocols favoring apoptosis are recommended when PDT is applied for curative treatment of *in situ* neoplasia. However, the induction of necrosis, accompanied by an inflammatory reaction, has been reported as a good option for curing infiltrative tumors.[144] The PDT activity obtained here is comparable to that described for HYP entrapped in glyconanoparticles, which afforded cell viability in the range 20-50%.[102]

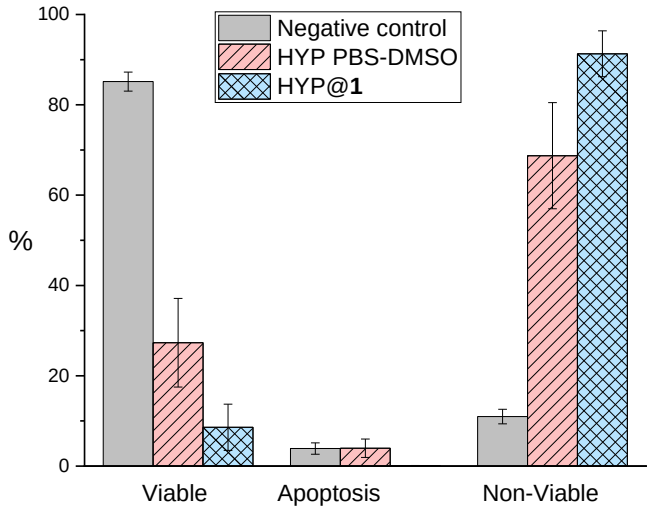

Figure 8. Results obtained by flow cytometry of cell viability and apoptosis in PDT experiments (2 min irradiation) with HT-29 cells and HYP as a photosensitizer. YO-PRO®-1/propidium iodide was used for staining. Negative control corresponds to cells incubated with PBS. The results are the average of three different batches analyzed in duplicate. [HYP] = 0.2 μM.

A relevant advantage of HYP@**1** over free HYP for their use in PDT is the avoidance of DMSO as a co-solvent. The use of solvents in cell cultures, commonly ethanol and DMSO, has some drawbacks that should not be neglected. For example, water-DMSO systems with 0.25 and 0.5% of the organic solvent induce inhibitory effects in some cell types and stimulatory impact in others.[145] Besides, the proportion of a co-solvent can change in biological media, causing HYP aggregation.

Finally, the study of photogeneration of $^1O_2$ in aqueous solutions of HYP@**1** by ABDA revealed that the photoactivity is similar to that of aggregated, poorly fluorescent, HYP in PBS control samples (kinetic constants of $1.9 \cdot 10^{-4}$ and $1.1 \cdot 10^{-4}$ s^{-1} respectively, see Figure S6). These results are in sharp contrast with the much more effective PDT observed in cells treated with HYP@**1** compared to those treated with HYP in PBS. A rationale for this behavior could be that encapsulation of HYP in the nanogel blocks significantly its action as a PDT agent, being the system activated for PDT upon intracellular nanogel disassembly. A similar effect was observed for the encapsulation of HYP in solid-lipid and polylactic acid-based nanoparticles.[96,137] Alternatively, it must be recalled that other ROS different from $^1O_2$ have been reported for HYP.[78] Hence, a more in-depth study would be needed to disclose which mechanism (type I or II), namely, which ROS ($^1O_2$ or $O_2^{\cdot -}$), is responsible for the observed PDT effects. The cytotoxic ability of $^1O_2$ has been linked to apoptotic changes,[146] while the impact of $O_2^{\cdot -}$ is more associated with lipid oxidation, altering membrane functions.[147] The different cell death mechanism observed for each ROS would reinforce the idea that the necrotic effects of HYP here reported are more likely due to $O_2^{\cdot -}$ at membranes than to $^1O_2$.

CONCLUSIONS

The use of non-polymeric, molecular, nanogels as vehicles for intracellular transport of actives has been hardly studied to date. Here, the nanogels formed by compound **1**, whose preparation and characterization were reported in a previous work,[24] show the capability of entrapping and promoting intracellular transport of two PDT agents, RB and HYP. These photosensitizers present markedly different physicochemical characteristics. RB is a dianionic species at neutral pH and water-soluble, while HYP is rather hydrophobic. These two compounds can be considered paradigmatic examples of substances that need vehicles for intracellular transport. The cellular membrane hinders the intracellular transport of anionic species like RB. At the same time, hydrophobic compounds such as HYP present such low solubility in plain water that their concentration in solution is not enough to be effective in PDT. Seemingly, the molecular nanogels can entrap HYP in the hydrophobic domains of the hydrogel particle, formed by self-assembled molecules of **1**. In contrast, in the case of RB, most likely adsorption through ion-dipole interactions with the polar units of the gel particle explains its incorporation. The mechanism of cellular uptake of the loaded nanogels is probably endocytosis considering the precedents in the literature but has not been studied in this work. Considering that hydrophobic interactions dominate the nanogel self-assembly, it seems feasible that the particles would be disassembled in the cellular medium upon, for example, interaction with proteins.

The results obtained by flow cytometry revealed an effective PDT action for both RB@**1** and HYP@**1** nanogels, showing no relevant dark toxicity confirming the biocompatibility of the delivery systems. The PDT efficiency compares well with previous reports using different nanocarriers. We believe that the use of nanogels described here presents an added value

coming from its molecular nature. Stimuli responsiveness of molecular particles would permit site-specific release/activation of the loaded species. Additionally, the molecular nature of the carrier should favor its biodispositon and avoid reproducibility and polydispersity issues associated with polymeric materials.

Finally, it is worth noting that the versatility of the nanogels could potentially permit simultaneous loading of PS and upconversion nanoparticles, affording IR-promoted PDT, a possibility that may be studied in future work.[42]

METHODS

Materials and general methods

Commercially available reagents and HPLC grade solvents were used as received and purchased from Sigma-Aldrich and Fisher Scientific unless otherwise stated. Phosphate buffered saline (PBS) tablets were used to prepare a PBS solution containing 0.01 M phosphate buffer, 0.0027 M potassium chloride, and 0.137 M sodium chloride. The pH was adjusted to 7.0, and the solution was filtered using a 0.22 μm pore nylon filter. Toluene was also filtered through a 0.45 μm pore nylon filter. MiliQ water was always used. Rose Bengal was used as the sodium dianionic form. Hypericin was obtained from HWL ANALYTIC GmbH. The solutions containing the photosensitizers were protected from light to avoid photobleaching.

Sonication was carried out with Elmasonic S 60 H (Elma) or Fisherbrand FB15053 (Fisher Scientific) ultrasonic units. Centrifugation was performed in vials using a Hettich EBA 20 centrifuge at room temperature or in Eppendorf tubes (1.5 mL) using a Beckman Coulter *Allegra*™ X-22R centrifuge at 15 ^{o}C.

UV-vis absorption spectra of the samples were recorded using a JASCO V-630 spectrophotometer with an ETCS-761 Peltier unit for temperature control. Measurements were performed at 25 ºC, and samples were loaded into 1.5 mL or 3 mL quartz SUPRASIL™ cuvettes, 10 mm optical path length, from Hellma Analytics.

Fluorescence emission spectra were obtained using a JASCO FP-8300 spectrofluorometer equipped with an ETC-815 Peltier accessory. Measurements were performed at 25 ºC, and samples were loaded into 3 mL optical glass cuvettes, 10 mm optical path length, Hellma Analytics.

Size measurements of nanogels were performed by dynamic light scattering (DLS) using a Zetasizer Nano ZS (Malvern). Analyses were carried out using a He-Ne laser (633 nm) at a fixed scattering angle of 173º. Automatic optimization of beam focusing and attenuation was applied for each sample. Nanogel suspensions were measured in 3 mL disposable PMMA cuvettes (10 mm optical path length). The particle size was reported as the average of three measurements. Z-potential measurements were performed at 25 ºC using Laser Doppler Micro-electrophoresis with a Zetasizer Nano ZS (Malvern). 1 mL of nanogels suspension was measured in disposable folded capillary zeta cells (Malvern, DTS1070). Z-potential is reported as the average of six measures per sample.

Synthesis of (*S*)-4-((3-methyl-1-(nonylamino)-1-oxobutan-2-yl)amino)-4-oxobutanoic acid (1) and nanogel preparation

The preparation of **1** and a detailed study of nanogel formation have been reported previously.[24]

Rose Bengal@1 (RB@1) preparation

In a typical example, 7.3 μmol of compound **1** and 1 mL of a 40 μM RB suspension in toluene (well dispersed by sonication and prepared from a 500 μM stock of RB) were introduced in a screw-capped vial (4 mL, diameter = 1.3 cm). A pink toluene gel with RB homogeneously dispersed was obtained after heating (heat gun, 250 ^{o}C) until complete solution and cooling down to room temperature in a water bath. The solvent from the gel was evaporated in a vacuum oven at 75 ^{o}C for 1 h. Then the xerogel was hydrated in 2 mL of PBS for 10 min. The suspension was ultrasonicated for 10 min and large particles were removed by centrifugation at 6000 rpm for 60 min to yield RB@**1** sample as the supernatant. The amount of RB in the sample was quantified by measuring the absorbance of RB and comparing the intensity at the λ_{max} with a calibration curve at 549 nm of RB solutions in PBS constructed for the range of concentration of interest. The procedure could be scaled up to prepare samples of RB@**1** of 7 mL with a similar concentration of RB@**1**. For control experiments, RB solutions in PBS were used in the same range of concentrations of that calculated for RB in the RB@**1** samples.

Hypericin@1 preparation

In a typical example, 7.3 μmol of compound **1** and 1 mL of 50 μM HYP suspension in toluene (well dispersed by sonication) were introduced in a screw-capped vial (4 mL, diameter = 1.3 cm). Then, the same protocol used for the preparation of RB@**1** was followed. The amount of HYP in the samples was quantified by measuring the absorbance of HYP and comparing the intensity at the λ_{max} with a calibration curve at 599 nm of HYP solutions in DMSO built for the range of concentrations of interest. The procedure could be scaled up to prepare samples of HYP@**1** of 7 mL with a similar concentration of HYP@**1**. For control experiments, HYP solutions at the same concentration than in HYP@**1** samples were

prepared in PBS containing a 1 % v/v DMSO (HYP in PBS-DMSO). HYP in PBS controls were prepared following HYP@**1** protocol without **1**.

Measurement of $^1O_2$ photogeneration

Samples with a total volume of 2 mL were placed in a 10 x 10 mm fluorescence quartz cuvette containing ABDA 1 μM as a $^1O_2$ probe (9,10-anthracenediyl-bis (methylene)dimalonic acid).), (from a 0.625 mM solution in methanol). Oxygen was bubbled through the solution, and the cuvette was closed with a stopper and Parafilm. The sample was then irradiated, under continuous stirring, with visible light using a LED light for the RB study (8.6 W, *ca.* 400-700 nm emission output, the lamp placed as closest to the cuvette as possible) and two LED lamps for the HYP study (11 W each one, *ca.* 400-700 nm emission output, the lamps placed perpendicular to each other at 1 cm from the cuvette). The cuvette was protected from external light during the process. The evolution of the photoreaction was monitored over time by fluorescence spectroscopy (λ_{ex} 380 nm), following the decrease of ABDA emission intensity at 407 nm. The initial points of the kinetic traces were fitted to a pseudo-first-order model ($\ln C/C_0 = - k_{obs} \times t$, where C is the concentration of ABDA at a specific time t and C_0 is the initial concentration of ABDA).

General considerations of biological assays

Human colon adenocarcinoma (HT-29) cell line was obtained from the American Type Culture Collection (ATCC). Cell culture media were purchased from Gibco (Thermo Fisher Scientific). Fetal bovine serum (FBS) was obtained from Harlan-Seralab. Supplements and other chemicals not listed in this section were obtained from Sigma-Aldrich. Plastics for cell culture were supplied by Thermo Fisher Scientific. Chambered coverslips from Ibidi were used for confocal microscopy.

HT-29 cell line was maintained in Dulbecco's modified Eagle's medium (DMEM) containing glucose (4.5 g/L), glutamine (2 mM), penicillin (50 µg/mL), streptomycin (50 µg/mL) and amphotericin B (1.25 µg/mL), supplemented with 10% FBS. Phenol red- or FBS-free medium with the same supplements were used when indicated to avoid fluorescence interferences or to promote starving conditions, respectively. Cells were grown at 37 ^{o}C in a 5% CO_2 humid atmosphere and, otherwise indicated, were also kept in these conditions during incubation. Sterilized PBS was used to wash or irradiate cells. Samples were tested in HT-29 cells in a 1:3 dilution with medium according to the results of the viability of the cells (using the Trypan blue staining method) after 24 h incubation with nanogels of **1** at different dilutions.

Flow cytometry analysis was performed with a BD Accuri^{TM} C6 flow cytometer. The data were recorded for at least 30,000 events per sample. When fluorescent probes were used, positive and negative populations were set up using an untreated or negative control cell population.

Confocal laser scanning microscopy (CLSM) analysis was performed on an inverted confocal microscope Leica TCS SP8. Images were obtained with an HC PL APO CS2 63x/1.40 oil immersion objective. Excitation of samples was performed with a diode laser excitation and fluorescence was acquired with a HyD detector, also recording the transmission.

Flow cytometry evaluation of the cellular uptake of loaded nanogels

HT-29 cells in a 6-/12-wells plate (60-70% confluence) were incubated for 24 h with the solutions to be tested (two replicas) in a 1:3 dilution with FBS-free and phenol red-free medium. After incubation, cells were harvested from the culture plates, washed three times with PBS, discarding the supernatant each time, and analyzed by flow cytometry. The

internalized probe was excited at 488 nm and the fluorescence emission per cell was measured using a 670LP filter for both RB and HYP. To be able to compare the data obtained between different experiments, results were normalized as the percentage of fluorescence intensity/cell over the negative control. Errors were obtained from the standard deviation of the duplicates and their transformation using partial derivatives based on the propagation of uncertainty.

Confocal microscopy evaluation of the cellular uptake of loaded nanogels

HT-29 cells in an µ-slide 8-wells Ibidi plate (60-70% confluence) were incubated overnight with the solutions to be tested in a 1:3 dilution with FBS-, phenol red-free medium. After washing four times with PBS, cells were kept in FBS-, phenol red-free medium, and visualized under the confocal microscope (RB: λ_{ex} = 514 nm, HYP: λ_{ex} 561 nm). The quantification of the fluorescence intensity of the cells was performed using ImageJ software, and results are expressed as the average fluorescence intensity/cell.

PDT assays

HT-29 cells in a 6-/12-wells plate (60-70% confluence) were incubated for 24 h with the solutions to be tested (two replicas) in a 1:3 dilution with phenol red-free medium. After incubation, cells were washed three times with PBS and, while kept in PBS, were irradiated for 2 min with two LED lamps (11 W each one, *ca.* 400-700 nm emission output) placed as close to the lid of the cells plate as possible resulting in an irradiance value of 750 Wm^{-2}. In non-irradiated controls, the plate was kept covered in aluminum foil under the same conditions. After another 24 h incubation in fresh phenol red-free medium, cells were washed with PBS and harvested. Afterward, cells were stained and analyzed by flow cytometry according to the instructions of the corresponding apoptosis detection kit:the FITC Annexin V apoptosis detection kit I (BD Pharmingen™, 556547) for RB and the YO-PRO®-

1/Propidium Iodide Vybrant™ Apoptosis Assay Kit #4 (V13243 Invitrogen ThermoFisher) for HYP. Cells populations were classified into viable (FITC Annexin V/YO-PRO®-1 and PI negative), apoptotic (FITC Annexin V/YO-PRO®-1 positive and PI negative), and non-viable cells (PI-positive).[148]

AUTHOR INFORMATION

Corresponding Author

*francisco.galindo@uji.es; miravet@uji.es

Author Contributions

The manuscript was written through the contributions of all authors. All authors have given approval to the final version of the manuscript.

ACKNOWLEDGMENT

Ministerio de Economía y Competitividad of Spain (grants CTQ2015-71004-R and RTI2018-101675-B-I00) and Universitat Jaume I (grant UJI-B2018-54) are thanked for financial support. A.T.-M. thanks Ministerio de Educación, Cultura y Deporte of Spain for a FPU fellowship (FPU14/05974). Technical support from SCIC of Universitat Jaume I is acknowledged.

ASSOCIATED CONTENT

Supporting Information. Cell viability obtained for non-irradiated control experiments and unloaded nanogel samples. Representative examples of the linear fit of ABDA. UV-Vis absorption spectra of HYP in DMSO and PBS. Additonal images of confocal laser scanning microscopy.

REFERENCES

(1) Shi, J.; Kantoff, P. W.; Wooster, R.; Farokhzad, O. C. Cancer nanomedicine: progress, challenges and opportunities. *Nat. Rev. Cancer* **2017**, *17*, 20-37.

(2) Pelaz, B.; Alexiou, C.; Alvarez-Puebla, R. A.; Alves, F.; Andrews, A. M.; Ashraf, S.; Balogh, L. P.; Ballerini, L.; Bestetti, A.; Brendel, C. *et al.* Diverse Applications of Nanomedicine. *ACS Nano* **2017**, *11*, 2313-2381.

(3) Pattni, B. S.; Chupin, V. V.; Torchilin, V. P. New Developments in Liposomal Drug Delivery. *Chem. Rev.* **2015**, *115*, 10938-10966.

(4) Tapeinos, C.; Battaglini, M.; Ciofani, G. Advances in the design of solid lipid nanoparticles and nanostructured lipid carriers for targeting brain diseases. *J. Control. Release* **2017**, *264*, 306-332.

(5) Kesharwani, S. S.; Kaur, S.; Tummala, H.; Sangamwar, A. T. Overcoming multiple drug resistance in cancer using polymeric micelles. *Expert Opin. Drug Deliv.* **2018**, *15*, 1127-1142.

(6) Mauri, E.; Perale, G.; Rossi, F. Nanogel Functionalization: A Versatile Approach To Meet the Challenges of Drug and Gene Delivery. *ACS Appl. Nano Mater.* **2018**, *1*, 6525-6541.

(7) Ekladious, I.; Colson, Y. L.; Grinstaff, M. W. Polymer–drug conjugate therapeutics: advances, insights and prospects. *Nat. Rev. Drug Discov.* **2019**, *18*, 273-294.

(8) Bhushan, B.; Khanadeev, V.; Khlebtsov, B.; Khlebtsov, N.; Gopinath, P. Impact of albumin based approaches in nanomedicine: Imaging, targeting and drug delivery. *Adv. Colloid Interface Sci.* **2017**, *246*, 13-39.

(9) Baeza, A.; Colilla, M.; Vallet-Regí, M. Advances in mesoporous silica nanoparticles for targeted stimuli-responsive drug delivery. *Expert Opin. Drug Deliv.* **2015**, *12*, 319-337.

(10) Sun, J.; Wei, Q.; Zhou, Y.; Wang, J.; Liu, Q.; Xu, H. A systematic analysis of FDA-approved anticancer drugs. *BMC Syst. Biol.* **2017**, *11*, 87.

(11) Bobo, D.; Robinson, K. J.; Islam, J.; Thurecht, K. J.; Corrie, S. R. Nanoparticle-Based Medicines: A Review of FDA-Approved Materials and Clinical Trials to Date. *Pharm. Res.* **2016**, *33*, 2373-2387.

(12) Hamidi, M.; Azadi, A.; Rafiei, P. Hydrogel nanoparticles in drug delivery. *Adv. Drug Deliv. Rev.* **2008**, *60*, 1638-1649.

(13) Oh, J. K.; Drumright, R.; Siegwart, D. J.; Matyjaszewski, K. The development of microgels/nanogels for drug delivery applications. *Prog. Polym. Sci.* **2008**, *33*, 448-477.

(14) Kabanov, A. V.; Vinogradov, S. V. Nanogels as pharmaceutical carriers: Finite networks of infinite capabilities. *Angew. Chem. Int. Ed.* **2009**, *48*, 5418-5429.

(15) Chacko, R. T.; Ventura, J.; Zhuang, J.; Thayumanavan, S. Polymer nanogels: A versatile nanoscopic drug delivery platform. *Adv. Drug Deliv. Rev.* **2012**, *64*, 836-851.

(16) Soni, K. S.; Desale, S. S.; Bronich, T. K. Nanogels: An overview of properties, biomedical applications and obstacles to clinical translation. *J. Control. Release* **2016**, *240*, 109-126.

(17) Neamtu, I.; Rusu, A. G.; Diaconu, A.; Nita, L. E.; Chiriac, A. P. Basic concepts and recent advances in nanogels as carriers for medical applications. *Drug Deliv.* **2017**, *24*, 539-557.

(18) Vinogradov, S.; Batrakova, E.; Kabanov, A. Poly(ethylene glycol)-polyethyleneimine NanoGel(TM) particles: Novel drug delivery systems for antisense oligonucleotides. *Colloids Surf. B* **1999**, *16*, 291-304.

(19) Lupitskyy, R.; Minko, S. Robust synthesis of nanogel particles by an aggregation-crosslinking method. *Soft Matter* **2010**, *6*, 4396-4402.

(20) Rösler, A.; Vandermeulen, G. W. M.; Klok, H.-A. Advanced drug delivery devices via self-assembly of amphiphilic block copolymers. *Adv. Drug Deliv. Rev.* **2001**, *53*, 95-108.

(21) Akiyoshi, K.; Deguchi, S.; Tajima, H.; Nishikawa, T.; Sunamoto, J. Microscopic structure and thermoresponsiveness of a hydrogel nanoparticle by self-assembly of a hydrophobized polysaccharide. *Macromolecules* **1997**, *30*, 857-861.

(22) Thelu, H. V. P.; Albert, S. K.; Golla, M.; Krishnan, N.; Ram, D.; Srinivasula, S. M.; Varghese, R. Size controllable DNA nanogels from the self-assembly of DNA nanostructures through multivalent host–guest interactions. *Nanoscale* **2018**, *10*, 222-230.

(23) Torres-Martínez, A.; Angulo-Pachón, C. A.; Galindo, F.; Miravet, J. F. Liposome-Enveloped Molecular Nanogels. *Langmuir* **2019**, *35*, 13375-13381.

(24) Torres-Martínez, A.; Angulo-Pachón, C. A.; Galindo, F.; Miravet, J. F. In between molecules and self-assembled fibrillar networks: Highly stable nanogel particles from a low molecular weight hydrogelator. *Soft Matter* **2019**, *15*, 3565-3572.

(25) Felip-León, C.; Cejudo-Marín, R.; Peris, M.; Galindo, F.; Miravet, J. F. Sizing Down a Supramolecular Gel into Micro- and Nanoparticles. *Langmuir* **2017**, *33*, 10322-10328.

(26) Vinogradov, S. V. Nanogels in the race for drug delivery. *Nanomedicine* **2010**, *5*, 165-168.

(27) Draper, E. R.; Adams, D. J. Controlling the Assembly and Properties of Low-Molecular-Weight Hydrogelators. *Langmuir* **2019**, *35*, 6506-6521.

(28) Draper, E. R.; Adams, D. J. Low-Molecular-Weight Gels: The State of the Art. *Chem* **2017**, *3*, 390-410.

(29) Hirst, A. R.; Escuder, B.; Miravet, J. F.; Smith, D. K. High-tech applications of self-assembling supramolecular nanostructured gel-phase materials: From regenerative medicine to electronic devices. *Angew. Chem. Int. Ed.* **2008**, *47*, 8002-8018.

(30) Weiss, R. G. The Past, Present, and Future of Molecular Gels. What Is the Status of the Field, and Where Is It Going? *J. Am. Chem. Soc.* **2014**, *136*, 7519-7530.

(31) Tran, S.; DeGiovanni, P.-J.; Piel, B.; Rai, P. Cancer nanomedicine: a review of recent success in drug delivery. *Clin. Transl. Med.* **2017**, *6*, 44.

(32) Donohoe, C.; Senge, M. O.; Arnaut, L. G.; Gomes-da-Silva, L. C. Cell death in photodynamic therapy: From oxidative stress to anti-tumor immunity. *Biochim. Biophys. Acta Rev. Cancer* **2019**, *1872*.

(33) Triesscheijn, M.; Baas, P.; Schellens, J. H. M.; Stewart, F. A. Photodynamic therapy in oncology. *Oncologist* **2006**, *11*, 1034-1044.

(34) Sharman, W. M.; Allen, C. M.; Van Lier, J. E. Photodynamic therapeutics: Basic principles and clinical applications. *Drug Discov. Today* **1999**, *4*, 507-517.

(35) Dolmans, D. E. J. G. J.; Fukumura, D.; Jain, R. K. Photodynamic therapy for cancer. *Nat. Rev. Cancer* **2003**, *3*, 380.

(36) Sharman, W. M.; Van Lier, J. E.; Allen, C. M. Targeted photodynamic therapy via receptor mediated delivery systems. *Adv. Drug Deliv. Rev.* **2004**, *56*, 53-76.

(37) Ethirajan, M.; Chen, Y.; Joshi, P.; Pandey, R. K. The role of porphyrin chemistry in tumor imaging and photodynamic therapy. *Chem. Soc. Rev.* **2011**, *40*, 340-362.

(38) MacDonald, I. J.; Dougherty, T. J. Basic principles of photodynamic therapy. *J. Porphyrins Phthalocyanines* **2001**, *5*, 105-129.

(39) Foote, C. S. Definition of type I and type II photosensitized oxidation. *Photochem. Photobiol.* **1991**, *54*, 659-659.

(40) DeRosa, M. C.; Crutchley, R. J. Photosensitized singlet oxygen and its applications. *Coord. Chem. Rev.* **2002**, *233-234*, 351-371.

(41) Plaetzer, K.; Krammer, B.; Berlanda, J.; Berr, F.; Kiesslich, T. Photophysics and photochemistry of photodynamic therapy: Fundamental aspects. *Lasers Med. Sci.* **2009**, *24*, 259-268.

(42) Lucky, S. S.; Soo, K. C.; Zhang, Y. Nanoparticles in photodynamic therapy. *Chem. Rev.* **2015**, *115*, 1990-2042.

(43) Chen, G.; Roy, I.; Yang, C.; Prasad, P. N. Nanochemistry and Nanomedicine for Nanoparticle-based Diagnostics and Therapy. *Chem. Rev.* **2016**, *116*, 2826-2885.

(44) Tynga, I. M.; Abrahamse, H. Nano-mediated photodynamic therapy for cancer: Enhancement of cancer specificity and therapeutic effects. *Nanomaterials* **2018**, *8*.

(45) Yang, B.; Chen, Y.; Shi, J. Reactive oxygen species (ROS)-based nanomedicine. *Chem. Rev.* **2019**, *119*, 4881-4985.

(46) Rabiee, N.; Yaraki, M. T.; Garakani, S. M.; Garakani, S. M.; Ahmadi, S.; Lajevardi, A.; Bagherzadeh, M.; Rabiee, M.; Tayebi, L.; Tahriri, M. *et al.* Recent advances in porphyrin-based nanocomposites for effective targeted imaging and therapy. *Biomaterials* **2020**, *232*.

(47) Buchner, M.; García Calavia, P.; Muhr, V.; Kröninger, A.; Baeumner, A. J.; Hirsch, T.; Russell, D. A.; Marín, M. J. Photosensitiser functionalised luminescent upconverting nanoparticles for efficient photodynamic therapy of breast cancer cells. *Photochem. Photobiol. Sci.* **2019**, *18*, 98-109.

(48) Penon, O.; Marín, M. J.; Russell, D. A.; Pérez-García, L. Water soluble, multifunctional antibody-porphyrin gold nanoparticles for targeted photodynamic therapy. *J. Colloid Interface Sci.* **2017**, *496*, 100-110.

(49) Neckers, D. C. Rose Bengal. *J. Photochem. Photobiol. A* **1989**, *47*, 1-29.

(50) Redmond, R. W.; Gamlin, J. N. A compilation of singlet oxygen yields from biologically relevant molecules. *Photochem. Photobiol.* **1999**, *70*, 391-475.

(51) Lacombe, S.; Pigot, T. Materials for selective photo-oxygenation vs. photocatalysis: Preparation, properties and applications in environmental and health fields. *Catal. Sci. Technol.* **2016**, *6*, 1571-1592.

(52) Fabregat, V.; Burguete, M. I.; Luis, S. V.; Galindo, F. Improving photocatalytic oxygenation mediated by polymer supported photosensitizers using semiconductor quantum dots as 'light antennas'. *RSC Advances* **2017**, *7*, 35154-35158.

(53) Manoil, D.; Filieri, A.; Schrenzel, J.; Bouillaguet, S. Rose bengal uptake by E. faecalis and F. nucleatum and light-mediated antibacterial activity measured by flow cytometry. *J. Photochem. Photobiol. B, Biol.* **2016**, *162*, 258-265.

(54) Li, C.; Lin, F.; Sun, W.; Wu, F. G.; Yang, H.; Lv, R.; Zhu, Y. X.; Jia, H. R.; Wang, C.; Gao, G. *et al.* Self-Assembled Rose Bengal-Exopolysaccharide Nanoparticles for Improved Photodynamic Inactivation of Bacteria by Enhancing Singlet Oxygen Generation Directly in the Solution. *ACS Appl. Mater. Interfaces* **2018**, *10*, 16715-16722.

(55) Qin, J.; Kunda, N.; Qiao, G.; Calata, J. F.; Pardiwala, K.; Prabhakar, B. S.; Maker, A. V. Colon cancer cell treatment with rose bengal generates a protective immune response via immunogenic cell death. *Cell Death Dis.* **2017**, *8*.

(56) Vanerio, N.; Stijnen, M.; De Mol, B. A. J. M.; Kock, L. M. Biomedical Applications of Photo- and Sono-Activated Rose Bengal: A Review. *Photobiomodul. Photomed. Laser Surg.* **2019**, *37*, 383-394.

(57) Burguete, M. I.; Galindo, F.; Gavara, R.; Luis, S. V.; Moreno, M.; Thomas, P.; Russell, D. A. Singlet oxygen generation using a porous monolithic polymer supported photosensitizer: Potential application to the photodynamic destruction of melanoma cells. *Photochem. Photobiol. Sci.* **2009**, *8*, 37-44.

(58) Delprat, G. D.; Epstein, N. N.; Kerr, W. J. A new liver function test: The elimination of rose bengal when injected into the circulation of human subjects. *Arch. Intern. Med.* **1924**, *34*, 533-541.

(59) Doughty, M. J. Rose bengal staining as an assessment of ocular surface damage and recovery in dry eye disease-A review. *Cont. Lens Anterior Eye* **2013**, *36*, 272-280.

(60) Ross, M. I. Intralesional therapy with PV-10 (Rose Bengal) for in-transit melanoma. *J. Surg. Oncol.* **2014**, *109*, 314-319.

(61) Tsao, S.; Yao, M.; Tsao, H.; Henry, F. P.; Zhao, Y.; Kochevar, J. J.; Redmond, R. W.; Kochevar, I. E. Light-activated tissue bonding for excisional wound closure: A split-lesion clinical trial. *Br. J. Dermatol.* **2012**, *166*, 555-563.

(62) Reinhard, A.; Sandborn, W. J.; Melhem, H.; Bolotine, L.; Chamaillard, M.; Peyrin-Biroulet, L. Photodynamic therapy as a new treatment modality for inflammatory and infectious conditions. *Expert Rev. Clin. Immunol.* **2015**, *11*, 637-657.

(63) Croce, A. C.; Wyroba, E.; Bottiroli, G. Distribution and retention of rose bengal and disulphonated aluminium phthalocyanine: A comparative study in unicellular eukaryote. *J. Photochem. Photobiol., B* **1992**, *16*, 318-330.

(64) Fischer, E.; Varga, F. Hepatic storage and biliary excretion of rose bengal in the rat. *Acta Physiol. Acad. Sci. Hung.* **1980**, *54*, 89-94.

(65) Calixto, G. M. F.; Bernegossi, J.; De Freitas, L. M.; Fontana, C. R.; Chorilli, M.; Grumezescu, A. M. Nanotechnology-based drug delivery systems for photodynamic therapy of cancer: A review. *Molecules* **2016**, *21*.

(66) Sztandera, K.; Gorzkiewicz, M.; Klajnert-Maculewicz, B. Nanocarriers in photodynamic therapy—in vitro and in vivo studies. *WIREs Nanomed Nanobiotechnol.* **2019**, e1509.

(67) Uppal, A.; Jain, B.; Gupta, P. K.; Das, K. Photodynamic Action of Rose Bengal Silica Nanoparticle Complex on Breast and Oral Cancer Cell Lines. *Photochem. Photobiol.* **2011**, *87*, 1146-1151.

(68) Dabrzalska, M.; Janaszewska, A.; Zablocka, M.; Mignani, S.; Majoral, J. P.; Klajnert-Maculewicz, B. Cationic Phosphorus Dendrimer Enhances Photodynamic Activity of Rose Bengal against Basal Cell Carcinoma Cell Lines. *Molecular Pharmaceutics* **2017**, *14*, 1821-1830.

(69) Wang, B.; Wang, J. H.; Liu, Q.; Huang, H.; Chen, M.; Li, K.; Li, C.; Yu, X. F.; Chu, P. K. Rose-bengal-conjugated gold nanorods for invivo photodynamic and photothermal oral cancer therapies. *Biomaterials* **2014**, *35*, 1954-1966.

(70) Gianotti, E.; Martins Estevão, B.; Cucinotta, F.; Hioka, N.; Rizzi, M.; Renò, F.; Marchese, L. An Efficient Rose Bengal Based Nanoplatform for Photodynamic Therapy. *Chem. Eur. J.* **2014**, *20*, 10921-10925.

(71) Wang, X. L.; Zeng, Y.; Zheng, Y. Z.; Chen, J. F.; Tao, X.; Wang, L. X.; Teng, Y. Rose bengal-grafted biodegradable microcapsules: Singlet-oxygen generation and cancer-cell incapacitation. *Chem. Eur. J.* **2011**, *17*, 11223-11229.

(72) Chaudhuri, S.; Sardar, S.; Bagchi, D.; Dutta, S.; Debnath, S.; Saha, P.; Lemmens, P.; Pal, S. K. Photoinduced Dynamics and Toxicity of a Cancer Drug in Proximity of Inorganic Nanoparticles under Visible Light. *ChemPhysChem* **2016**, *17*, 270-277.

(73) Sabri, T.; Pawelek, P. D.; Capobianco, J. A. Dual Activity of Rose Bengal Functionalized to Albumin-Coated Lanthanide-Doped Upconverting Nanoparticles: Targeting and Photodynamic Therapy. *ACS Appl. Mater. Interfaces* **2018**, *10*, 26947-26953.

(74) Karthikeyan, K.; Babu, A.; Kim, S. J.; Murugesan, R.; Jeyasubramanian, K. Enhanced photodynamic efficacy and efficient delivery of Rose Bengal using nanostructured

poly(amidoamine) dendrimers: Potential application in photodynamic therapy of cancer. *Cancer Nanotechnol.* **2011**, *2*, 95-103.

(75) Waser, M.; Falk, H. Progress in the chemistry of second generation Hypericin based Photosensitizers. *Curr. Org. Chem.* **2011**, *15*, 3894-3907.

(76) Jendželovská, Z.; Jendželovský, R.; Kuchárová, B.; Fedoročko, P. Hypericin in the Light and in the Dark: Two Sides of the Same Coin. *Front. Plant Sci.* **2016**, *7*.

(77) Diwu, Z.; William Lown, J. Photosensitization with anticancer agents 17. EPR studies of photodynamic action of hypericin: Formation of semiquinone radical and activated oxygen species on illumination. *Free Radical Biol. Med.* **1993**, *14*, 209-215.

(78) López-Chicón, P.; Paz-Cristobal, M. P.; Rezusta, A.; Aspiroz, C.; Royo-Cañas, M.; Andres-Ciriano, E.; Gilaberte, Y.; Agut, M.; Nonell, S. On the mechanism of Candida spp. photoinactivation by hypericin. *Photochem. Photobiol. Sci.* **2012**, *11*, 1099-1107.

(79) Agostinis, P.; Vantieghem, A.; Merlevede, W.; De Witte, P. A. M. Hypericin in cancer treatment: More light on the way. *Int. J. Biochem. Cell Biol.* **2002**, *34*, 221-241.

(80) Vandenbogaerde, A. L.; Cuveele, J. F.; Proot, P.; Himpens, B. E.; Merlevede, W. J.; De Witte, P. A. Differential cytotoxic effects induced after photosensitization by hypericin. *J. Photochem. Photobiol. B, Biol.* **1997**, *38*, 136-142.

(81) Noell, S.; Mayer, D.; Strauss, W. S. L.; Tatagiba, M. S.; Ritz, R. Selective enrichment of hypericin in malignant glioma: Pioneering in vivo results. *Int. J. Oncol.* **2011**, *38*, 1343-1348.

(82) Alecu, M.; Ursaciuc, C.; Hãlãlãu, F.; Coman, G.; Merlevede, W.; Waelkens, E.; De Witte, P. Photodynamic treatment of basal cell carcinoma and squamous cell carcinoma with hypericin. *Anticancer Res.* **1998**, *18*, 4651-4654.

(83) Kacerovská, D.; Pizinger, K.; Majer, F.; Šmíd, F. Photodynamic therapy of nonmelanoma skin cancer with topical Hypericum perforatum extract - A pilot study. *Photochem. Photobiol.* **2008**, *84*, 779-785.

(84) Rook, A. H.; Wood, G. S.; Duvic, M.; Vonderheid, E. C.; Tobia, A.; Cabana, B. A phase II placebo-controlled study of photodynamic therapy with topical hypericin and visible light irradiation in the treatment of cutaneous T-cell lymphoma and psoriasis. *J. Am. Acad. Dermatol.* **2010**, *63*, 984-990.

(85) Rezusta, A.; Lõpez-Chicõn, P.; Paz-Cristobal, M. P.; Alemany-Ribes, M.; Royo-Díez, D.; Agut, M.; Semino, C.; Nonell, S.; Revillo, M. J.; Aspiroz, C. *et al.* In vitro fungicidal photodynamic effect of hypericin on candida species. *Photochem. Photobiol.* **2012**, *88*, 613-619.

(86) García, I.; Ballesta, S.; Gilaberte, Y.; Rezusta, A.; Pascual, Á. Antimicrobial photodynamic activity of hypericin against methicillin-susceptible and resistant Staphylococcus aureus biofilms. *Future Microbiol.* **2015**, *10*, 347-356.

(87) Hudson, J. B.; Harris, L.; Towers, G. H. N. The importance of light in the anti-HIV effect of hypericin. *Antiviral Res.* **1993**, *20*, 173-178.

(88) Castano, A. P.; Demidova, T. N.; Hamblin, M. R. Mechanisms in photodynamic therapy: Part three - Photosensitizer pharmacokinetics, biodistribution, tumor localization and modes of tumor destruction. *Photodiagnosis Photodyn Ther.* **2005**, *2*, 91-106.

(89) Saw, C. L. L.; Olivo, M.; Soo, K. C.; Heng, P. W. S. Delivery of hypericin for photodynamic applications. *Cancer Letters* **2006**, *241*, 23-30.

(90) Bánó, G.; Staničová, J.; Jancura, D.; Marek, J.; Bánó, M.; Uličný, J.; Strejčková, A.; Miškovský, P. On the diffusion of hypericin in dimethylsulfoxide/water mixtures-the effect of aggregation. *J. Phys. Chem. B* **2011**, *115*, 2417-2423.

(91) Falk, H. From the photosensitizer hypericin to the photoreceptor stentorin - The chemistry of phenantroperylene quinones. *Angew. Chem. Int. Ed.* **1999**, *38*, 3117-3136.

(92) Lajos, G.; Jancura, D.; Miskovsky, P.; García-Ramos, J. V.; Sanchez-Cortes, S. Surface-enhanced fluorescence and raman scattering study of antitumoral drug hypericin: An effect of aggregation and self-spacing depending on pH. *J. Phys. Chem. C* **2008**, *112*, 12974-12980.

(93) Theodossiou, T.; Spiro, M. D.; Jacobson, J.; Hothersall, J. S.; MacRobert, A. J. Evidence for intracellular aggregation of hypericin and the impact on its photocytotoxicity in PAM 212 murine keratinocytes. *Photochem. Photobiol.* **2004**, *80*, 438-443.

(94) Zeisser-Labouèbe, M.; Delie, F.; Gurny, R.; Lange, N. Benefits of nanoencapsulation for the hypercin-mediated photodetection of ovarian micrometastases. *Eur. J. Pharm. Biopharm.* **2009**, *71*, 207-213.

(95) Mondon, K.; Zeisser-Labouèbe, M.; Gurny, R.; Möller, M. MPEG-hexPLA micelles as novel carriers for hypericin, a fluorescent marker for use in cancer diagnostics. *Photochem. Photobiol.* **2011**, *87*, 399-407.

(96) Lima, A. M.; Pizzol, C. D.; Monteiro, F. B. F.; Creczynski-Pasa, T. B.; Andrade, G. P.; Ribeiro, A. O.; Perussi, J. R. Hypericin encapsulated in solid lipid nanoparticles: Phototoxicity and photodynamic efficiency. *J. Photochem. Photobiol. B, Biol.* **2013**, *125*, 146-154.

(97) Nafee, N.; Youssef, A.; El-Gowelli, H.; Asem, H.; Kandil, S. Antibiotic-free nanotherapeutics: Hypericin nanoparticles thereof for improved in vitro and in vivo antimicrobial photodynamic therapy and wound healing. *Int. J. Pharm.* **2013**, *454*, 249-258.

(98) Lopera, A. A.; Montoya, A.; Vélez, I. D.; Robledo, S. M.; Garcia, C. P. Synthesis of calcium phosphate nanostructures by combustion in solution as a potential encapsulant

system of drugs with photodynamic properties for the treatment of cutaneous leishmaniasis. *Photodiagnosis Photodyn Ther.* **2018**, *21*, 138-146.

(99) Delcanale, P.; Rodríguez-Amigo, B.; Juárez-Jiménez, J.; Luque, F. J.; Abbruzzetti, S.; Agut, M.; Nonell, S.; Viappiani, C. Tuning the local solvent composition at a drug carrier surface: the effect of dimethyl sulfoxide/water mixture on the photofunctional properties of hypericin-β-lactoglobulin complexes. *J. Mater. Chem. B* **2017**, *5*, 1633-1641.

(100) Delcanale, P.; Pennacchietti, F.; Maestrini, G.; Rodríguez-Amigo, B.; Bianchini, P.; Diaspro, A.; Iagatti, A.; Patrizi, B.; Foggi, P.; Agut, M. *et al.* Subdiffraction localization of a nanostructured photosensitizer in bacterial cells. *Sci. Rep.* **2015**, *5*.

(101) Han, C.; Zhang, C.; Ma, T.; Zhang, C.; Luo, J.; Xu, X.; Zhao, H.; Chen, Y.; Kong, L. Hypericin-functionalized graphene oxide for enhanced mitochondria-targeting and synergistic anticancer effect. *Acta Biomater.* **2018**, *77*, 268-281.

(102) Shao, C.; Shang, K.; Xu, H.; Zhang, Y.; Pei, Z.; Pei, Y. Facile fabrication of hypericin-entrapped glyconanoparticles for targeted photodynamic therapy. *Int. J. Nanomedicine* **2018**, *13*, 4319-4331.

(103) Josefsen, L. B.; Boyle, R. W. Photodynamic therapy: novel third-generation photosensitizers one step closer? *Br. J. Pharmacol.* **2008**, *154*, 1-3.

(104) Muehlmann, L. A.; Ma, B. C.; Longo, J. P. F.; Almeida Santos, M. F. M.; Azevedo, R. B. Aluminum-phthalocyanine chloride associated to poly(methyl vinyl ether-co-maleic anhydride) nanoparticles as a new third-generation photosensitizer for anticancer photodynamic therapy. *Int. J. Nanomedicine* **2014**, *9*, 1199-1213.

(105) Konan, Y. N.; Gurny, R.; Allémann, E. State of the art in the delivery of photosensitizers for photodynamic therapy. *J. Photochem. Photobiol. B, Biol.* **2002**, *66*, 89-106.

(106) Arnau-del-Valle, C.; Felip-León, C.; Angulo-Pachón, C. A.; Galindo, F.; Miravet, J. F. Adsorption of Rose Bengal on a self-assembled fibrillar network affords a thermally switchable oxygenation photocatalyst and a thermochromic soft material. *J. Photochem. Photobiol. A* **2020**, *387*.

(107) Pereira, P. C. D. S.; Costa, P. F. D. A.; Pellosi, D. S.; Calori, I. R.; Vilsinski, B. H.; Estevão, B. M.; Hioka, N.; Caetano, W. Photophysical properties and interaction studies of Rose Bengal derivatives with biomimetic systems based in micellar aqueous solutions. *J. Mol. Liq.* **2017**, *230*, 674-685.

(108) Bhowmik, B. B.; Ganguly, P. Photophysics of xanthene dyes in surfactant solution. *Spectrochim. Acta A* **2005**, *61*, 1997-2003.

(109) Chang, C. C.; Yang, Y. T.; Yang, J. C.; Wu, H. D.; Tsai, T. Absorption and emission spectral shifts of rose bengal associated with DMPC liposomes. *Dyes and Pigments* **2008**, *79*, 170-175.

(110) Fadel, M.; Kassab, K. Evaluation of the photostability and photodynamic efficacy of Rose Bengal loaded in multivesicular liposomes. *Trop. J. Pharm. Res.* **2011**, *10*, 289-297.

(111) Lee, J. S.; Lee, B. I.; Park, C. B. Photo-induced inhibition of Alzheimer's β-amyloid aggregation invitro by rose Bengal. *Biomaterials* **2015**, *38*, 43-49.

(112) Alarcon, E. I.; Poblete, H.; Roh, H.; Couture, J. F.; Comer, J.; Kochevar, I. E. Rose Bengal binding to collagen and tissue photobonding. *ACS Omega* **2017**, *2*, 6646-6657.

(113) Fabregat, V.; Burguete, M. I.; Galindo, F.; Luis, S. V. Singlet oxygen generation by photoactive polymeric microparticles with enhanced aqueous compatibility. *Environ. Sci. Pollut. Res. Int.* **2014**, *21*, 11884-11892.

(114) Arbeloa, E. M.; Previtali, C. M.; Bertolotti, S. G. A Comparative Study on the Photophysics and Photochemistry of Xanthene Dyes in the Presence of Polyamidoamine (PAMAM) Dendrimers. *ChemPhysChem* **2018**, *19*, 934-942.

(115) Valdes-Aguilera, O.; Neckers, D. C. Rose bengal ethyl ester aggregation in aqueous solution. *J. Phys. Chem.* **1988**, *92*, 4286-4289.

(116) Swift, L.; Zhang, C.; Trippett, T.; Narendran, A. Potent in vitro and xenograft antitumor activity of a novel agent, PV-10, against relapsed and refractory neuroblastoma. *OncoTargets Ther.* **2019**, *12*, 1293-1307.

(117) Kochevar, I. E.; Bouvier, J.; Lynch, M.; Chi-Wei, L. Influence of dye and protein location on photosensitization of the plasma membrane. *Biochim. Biophys. Acta* **1994**, *1196*, 172-180.

(118) Valenzeno, D. P.; Trudgen, J.; Hutzenbuhler, A.; Milne, M. Singlet oxygen involvement in photohemolysis sensitized by merocyanine-540 and rose bengal *Photochem. Photobiol.* **1987**, *46*, 985-990.

(119) Wieder, M. E.; Hone, D. C.; Cook, M. J.; Handsley, M. M.; Gavrilovic, J.; Russell, D. A. Intracellular photodynamic therapy with photosensitizer-nanoparticle conjugates: Cancer therapy using a 'Trojan horse'. *Photochem. Photobiol. Sci.* **2006**, *5*, 727-734.

(120) Sahay, G.; Alakhova, D. Y.; Kabanov, A. V. Endocytosis of nanomedicines. *J. Control. Release* **2010**, *145*, 182-195.

(121) Proskuryakov, S. Y.; Konoplyannikov, A. G.; Gabai, V. L. Necrosis: A specific form of programmed cell death? *Exp. Cell Res.* **2003**, *283*, 1-16.

(122) Abrams, J.; G.Telford, W.; Rollins, L. The many roads to cell death: Discriminating between apoptosis, necrosis and autophagy. *Drug Discov. World* **2014**, *16*, 41-46.

(123) Fuchs, Y.; Steller, H. Live to die another way: Modes of programmed cell death and the signals emanating from dying cells. *Nat. Rev. Mol. Cell Biol.* **2015**, *16*, 329-344.

(124) Nikoletopoulou, V.; Markaki, M.; Palikaras, K.; Tavernarakis, N. Crosstalk between apoptosis, necrosis and autophagy. *Biochim. Biophys. Acta, Mol. Cell Res.* **2013**, *1833*, 3448-3459.

(125) Kessel, D. Apoptosis, Paraptosis and Autophagy: Death and Survival Pathways Associated with Photodynamic Therapy. *Photochem. Photobiol.* **2019**, *95*, 119-125.

(126) Castano, A. P.; Demidova, T. N.; Hamblin, M. R. Mechanisms in photodynamic therapy: Part one - Photosensitizers, photochemistry and cellular localization. *Photodiagnosis Photodyn Ther.* **2004**, *1*, 279-293.

(127) Castano, A. P.; Demidova, T. N.; Hamblin, M. R. Mechanisms in photodynamic therapy: Part two - Cellular signaling, cell metabolism and modes of cell death. *Photodiagnosis Photodyn Ther.* **2005**, *2*, 1-23.

(128) Panzarini, E.; Inguscio, V.; Dini, L. Timing the multiple cell death pathways initiated by Rose Bengal acetate photodynamic therapy. *Cell Death Dis.* **2011**, *2*.

(129) Felip-León, C.; Puche, M.; Miravet, J. F.; Galindo, F.; Feliz, M. A spectroscopic study to assess the photogeneration of singlet oxygen by graphene oxide. *Mater. Lett.* **2019**, *251*, 45-51.

(130) Hackbarth, S.; Röder, B. Singlet oxygen luminescence kinetics in a heterogeneous environment – identification of the photosensitizer localization in small unilamellar vesicles. *Photochem. Photobiol. Sci.* **2015**, *14*, 329-334.

(131) Joniova, J.; Rebič, M.; Strejčková, A.; Huntosova, V.; Staničová, J.; Jancura, D.; Miskovsky, P.; Bánó, G. Formation of Large Hypericin Aggregates in Giant Unilamellar Vesicles—Experiments and Modeling. *Biophys. J.* **2017**, *112*, 966-975.

(132) Barras, A.; Skandrani, N.; Gonzalez Pisfil, M.; Paryzhak, S.; Dumych, T.; Haustrate, A.; Héliot, L.; Gharbi, T.; Boulahdour, H.; Lehen'kyi, V. *et al.* Improved photodynamic effect through encapsulation of two photosensitizers in lipid nanocapsules. *J. Mater. Chem. B* **2018**, *6*, 5949-5963.

(133) Penjweini, R.; Deville, S.; D'Olieslaeger, L.; Berden, M.; Ameloot, M.; Ethirajan, A. Intracellular localization and dynamics of Hypericin loaded PLLA nanocarriers by image correlation spectroscopy. *J. Control. Release* **2015**, *218*, 82-93.

(134) Barras, A.; Boussekey, L.; Courtade, E.; Boukherroub, R. Hypericin-loaded lipid nanocapsules for photodynamic cancer therapy in vitro. *Nanoscale* **2013**, *5*, 10562-10572.

(135) Yamazaki, T.; Ohta, N.; Yamazaki, I.; Song, P. S. Excited-state properties of hypericin: Electronic spectra and fluorescence decay kinetics. *J. Phys. Chem.* **1993**, *97*, 7870-7875.

(136) Cheng, W.; Fan, F.; Zhang, Y.; Pei, Z.; Wang, W.; Pei, Y. A facile approach for fabrication of core-shell magnetic molecularly imprinted nanospheres towards hypericin. *Polymers* **2017**, *9*.

(137) Zeisser-Labouèbe, M.; Mattiuzzo, M.; Lange, N.; Gurny, R.; Delie, F. Quenching-induced deactivation of photosensitizer by nanoencapsulation to improve phototherapy of cancer. *J. Drug Target.* **2009**, *17*, 619-626.

(138) Fadel, M.; Kassab, K.; Youssef, T. Photodynamic efficacy of hypericin targeted by two delivery techniques to hepatocellular carcinoma cells. *Lasers Med. Sci.* **2010**, *25*, 675-683.

(139) Huntosova, V.; Buzova, D.; Petrovajova, D.; Kasak, P.; Nadova, Z.; Jancura, D.; Sureau, F.; Miskovsky, P. Development of a new LDL-based transport system for hydrophobic/amphiphilic drug delivery to cancer cells. *Int. J. Pharm.* **2012**, *436*, 463-471.

(140) de Morais, F. A. P.; Gonçalves, R. S.; Vilsinski, B. H.; de Oliveira, L.; Rocha, N. L.; Hioka, N.; Caetano, W. Hypericin photodynamic activity in DPPC liposome. PART I:

biomimetism of loading, location, interactions and thermodynamic properties. *J. Photochem. Photobiol. B, Biol.* **2019**, *190*, 118-127.

(141) Ali, S. M.; Olivo, M. Bio-distribution and subcellular localization of Hypericin and its role in PDT induced apoptosis in cancer cells. *Int. J. Oncol.* **2002**, *21*, 531-540.

(142) Vuong, T. T. K.; Vever-Bizet, C.; Bonneau, S.; Bourg-Heckly, G. Hypericin incorporation and localization in fixed HeLa cells for various conditions of fixation and incubation. *Photochem. Photobiol. Sci.* **2011**, *10*, 561-568.

(143) Mikeš, J.; Kleban, J.; Sačková, V.; Horváth, V.; Jamborová, E.; Vaculová, A.; Kozubík, A.; Hofmanová, J.; Fedoročko, P. Necrosis predominates in the cell death of human colon adenocarcinoma HT-29 cells treated under variable conditions of photodynamic therapy with hypericin. *Photochem. Photobiol. Sci.* **2007**, *6*, 758-766.

(144) Marchal, S.; Fadloun, A.; Maugain, E.; D'Hallewin, M. A.; Guillemin, F.; Bezdetnaya, L. Necrotic and apoptotic features of cell death in response to Foscan® photosensitization of HT29 monolayer and multicell spheroids. *Biochem. Pharmacol.* **2005**, *69*, 1167-1176.

(145) Timm, M.; Saaby, L.; Moesby, L.; Hansen, E. W. Considerations regarding use of solvents in in vitro cell based assays. *Cytotechnology* **2013**, *65*, 887-894.

(146) Kochevar, I. E.; Lynch, M. C.; Zhuang, S.; Lambert, C. R. Singlet oxygen, but not oxidizing radicals, induces apoptosis in HL-60 cells. *Photochem. Photobiol.* **2000**, *72*, 548-553.

(147) Kochevar, I. E.; Lambert, C. R.; Lynch, M. C.; Tedesco, A. C. Comparison of photosensitized plasma membrane damage caused by singlet oxygen and free radicals. *Biochimica et Biophysica Acta - Biomembranes* **1996**, *1280*, 223-230.

(148) Glisic-Milosavljevic, S.; Waukau, J.; Jana, S.; Jailwala, P.; Rovensky, J.; Ghosh, S. Comparison of apoptosis and mortality measurements in peripheral blood mononuclear cells (PBMCs) using multiple methods. *Cell Prolif.* **2005**, *38*, 301-311.

TOC graph

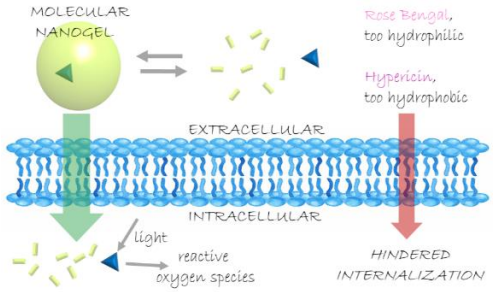
MOLECULAR
NANOGEL
Rose Bengal,
too hydrophilic
Hypericin,
too hydrophobic
EXTRACELLULAR
INTRACELLULAR
light
reactive
oxygen species
HINDERED
INTERNALIZATION